UDC 621.791.75:621.791.01:536.2:519.87
DOI: 10.15587/2706-5448.2026.352967

Adel Chouiter,
Lyes Bidi,
Hadjer Bensiali,
Rachid Chaib,
Philippe Le Masson

DEVELOPMENT OF A PREDICTIVE THERMAL MODEL BASED ON THE EQUIVALENT SOURCE APPROACH FOR SMAW WELDING OF X70 STEEL PIPES

The object of the research is the scientific approach for modeling thermal phenomena during welding operations in SMAW welding of pipelines. This model can be used to calculate changes in temperature fields as well as stresses and deformations.

Mastering welding processes requires an understanding of the various phenomena involved. This requires numerous tests to be carried out, which are very costly for manufacturers. The ideal solution would therefore be to develop predictive numerical models that would enable the behavior of assemblies to be analyzed. The SMAW process is used to fill a chamfer between two parts. It is therefore essential to define heat input, which can be described using the equivalent heat source approach the equivalent heat source approach. The difficulty in implementing this approach lies in estimating the various parameters of the model. To this end, it was proposed to develop a simple and robust approach, which consists of using the numerical design of experiments (NDE) method.

In this research, it was decided to select four parameters from the model (r_{surf_sup}, r_{surf_inf}, r_0 and λ) and four objective functions characterizing the shape of the fusion zone (L_{sup}, L_m, L_{inf}, H). Preliminary results show good agreement between the direct model and the dimensions recorded on the macrographic sections, with the exception of the width of the median side of the fusion zone (L_m), where there is a significant deviation of 11.4% between the measurements and the model. Furthermore, the NDE shows that r_{surf_inf} is the factor that most influences L_m. Adjusting the r_{surf_inf} factor by 0.5 from its value at the central point changes the L_m value from 3.25 mm to 3.09 mm. This adjustment optimizes the digital model by improving it and reducing the discrepancy between the simulation and the experiment for the L_m function from 11.4% to 1.2%. The results of this research make it possible to increase the reliability of petroleum facilities (pipeline assemblies). The scientific novelty of this research lies in the implementation of a simple and robust scientific approach for optimizing non-physical parameters (equivalent heat source parameters) in the modeling of welding processes.

Keywords: *welding simulation, numerical design, SMAW welding, equivalent heat source, adjustments parameters.*

Received: 06.12.2025
Received in revised form: 29.01.2026
Accepted: 20.02.2026
Published: 28.02.2026

How to cite
Chouiter, A., Bidi, L., Bensiali, H., Chaib, R., Le Masson, P. (2026). Development of a predictive thermal model based on the equivalent source approach for SMAW welding of X70 steel pipes. Technology Audit and Production Reserves, 1 (1 (87)), 6–14. https://doi.org/10.15587/2706-5448.2026.352967

1. Introduction

Joining by welding occupies an important part in the world of boat building, trains, rockets, cars, bridges, pipes, tanks and so many other things that would not be built without the use of welding. The aim is to ensure mechanical continuity between the parts to be joined with or without filler material allowing a better link between the parts. Nowadays, there are many welding processes available for the wide variety of assemblies to be made and the characteristics of the metals used. However, several phenomena involved in welding processes are multiple, coupled, and require a thorough understanding. Ideally, therefore, predictive numerical models should be developed to analyze the behavior of assemblies during and after welding thus reducing the number of tests. The objective of numerical simulation of welding is generally to describe the mechanical effects (such as stress fields and distortions) which are directly dependent on the temperature changes imposed by the welding process. It is therefore imperative to access the definition of heat input which can be described according to two approaches: the multiphysics approach and the "equivalent source" approach. In this work, the equivalent source approach was chosen, because it is easy to implement it with an acceptable computation time. This approach generally involves solving a non-linear conduction problem in the parts to be joined. Our choice of sources is based on a combination of three types of equivalent sources. The first is a parietal Gaussian surface source on the top face, the second is a Gaussian volume source distributed in the thickness in a conical shape [1]. The third being a Gaussian surface source on the bottom side. Where experiments are deemed expensive, it is increasingly common to study phenomena first using numerical simulations. The calculations are often complex and require very long calculation times. It is then advantageous to organize the simulations in the same way as the experimental design tests. The usefulness of these numerical plans is on the one hand, to quantify the influence of the model parameters on the chosen objective functions, in order to minimize the number of parameters to be studied. And on the other hand, to try to find the range of input parameters of the model, so as to judge the robustness of the numerical model. In this work, three equivalent source parameters (r_{surf_sup}, r_{surf_inf}, r_0), thermal conductivity λ and four objective functions were chosen. These functions are the width of the upper part (L_{sup}), the width of the central part (L_m), the width of the lower part of the molten zone (L_{inf}) and the height of the

deposit on the chamfered walls (*H*). In the literature, there are several studies that address the modelling of welding operations. The thermal study based on the double ellipsoid heat source approach enables the calculation of temperature and residual stresses [2]. To thermally simulate GMAW laser welding, two types of heat sources are used: an ellipsoidal volumetric source to simulate the heat input of arc welding and a cylindrical volumetric source to simulate the heat input of the laser beam [3]. The temperature fields and stress fields in the case of multiple welding for medium-thickness plates are based on the heat source approach [4]. The combination of the equivalent heat source approach and the experimental design method makes it possible to determine the thermal field in hybrid laser-MIG welding [5]. The equivalent source approach enables the determination of thermal mapping, residual stresses and deformations for GTAW welding [6]. The simulation of heat transfer phenomena due to hybrid welding operations using the heat source method provides relevant numerical models [7]. Equivalent sources can use to model several welding processes such as: lap welding and circumferential welding (butt welding), in a carbon-manganese pipe coated by the TIG process [8]. They developed a numerical model using a double Goldak ellipsoid heat source [9]. A four-point heat source and two equivalent heat sources have been studied for narrow-gap multilayer rotary arc MAG welding in order to analyze the weld shape, stress distribution and the distortion in an average steel plate [10]. The heat source is described as a homogeneous heat flow and it allows the prediction of the main dimensions of the weld bead and the evolution of the temperature in the part [11]. Furthermore, heat source modelling can be used to solve the problem of hot cracking induced by residual stress in Inconel 738LC weld deposits [12]. For thermal modelling of welding operations, depending on the shape of the molten zone, it is possible to use not only a single heat source but also several at the same time [13]. The three-dimensional transient temperature field of TIG welding of CLAM steel with preheating was simulated. The simulation results were compared with those from infrared thermography measurements. These results are obtained at different welding speeds [14]. The new forms of heat sources are possible, depending on the type of welding process, such as: high-energy welding processes (laser, electron beam, etc.) and electric arc welding processes. The energy provided by laser beam welding can be described by a source volumetric heat source such as double-ellipsoidal [15]. The application of a double-ellipsoidal heat power density distribution is less appropriate for keyhole-laser or electron-beam welding operations. However, double ellipsoidal is extended to a double ellipsoidal-conical thermal power density model in order to accurately describe transient temperature fields for a wider range of welding geometries and processes [16]. In multilayer wading thanks to the hybrid laser-arc welding process, the equivalent source approach is used for multiphysics calculations [17]. Heat sources may have variable profiles for numerical modelling of different welding processes [18]. The modification of the double ellipsoid heat source allows for special shapes, such as the shape of an avocado [19]. Automating conventional steps can contribute to more efficient industrial use of FE simulation, facilitating the simulation of the welding process [20]. The temperature field during welding and the residual stress and deformation fields induced by welding are predicted by numerical simulation [21]. Some studies use model parameter optimization methods for global welding simulations (Levenberg-Marquardt neural network algorithm, etc.), mainly due to their high computational cost [22]. The calculation of temperature fields is an important step in the study of the thermal field of welding. Therefore, the accuracy of temperature measurement is very important to provide significant results and establish the coupling between the thermal field results and other welding studies, such as mechanical behavior [23]. The parameters of the equivalent heat source model have significant influence on the temperature field and sequentially affect the residual stress field and deformations [24]. The determination of the optimal heat source parameters is an important step in welding simulations using experimental results [25]. Ideally, the experimental results should be compared with the numerical ones, bearing in mind that this has been done by [26].

The object of the research is the scientific approach for modeling thermal phenomena during welding operations in SMAW welding of pipelines. This understanding allows for better control of the pipeline assembly process, resulting in higher quality weld beads.

The aim of this research is to propose a thermal model, both simple and relevant, allowing to find the temporal and spatial evolutions of the temperature of the two parts to be assembled, in the vicinity of the bead, during welding. This model will integrate it into a thermomechanical calculation in order to deduce the stresses and deformations.

To achieve the aim, it is necessary to complete such tasks:

1. To carry out experimental tests in order to approach the operating parameters validated by the macrographic analysis of the cross-sections of the weld beads. The work continues with a phenomenological analysis of welding with the aim of extracting as much information as possible in order to develop a numerical model representing the heat input based on the heat source approach. The numerical model can then be built under a numerical calculation code.
2. To compare theoretical and experimental macrographic sections, an optimal set of equivalent source parameters being known, a numerical experimental plan is implemented to analyze the behavior of the model with respect to the source parameters. The adjustment of the parameters of the digital model, to bring the calculated values closer to the measured values, is carried out using the effect diagrams, taking into account the amplitude and direction of the effects of the influence factors on the objective functions.
3. To adjusting the parameters of heat sources using the numerical design of experiments allows the optimum parameter sets to be found in order to maximize the relevance of the numerical model. A comparison between the shape of the experimental and numerical molten zone allows the validation of the model.

2. Materials and Methods

2.1. Description of the process implemented

Manual SMAW welding is used to join pipes of 1219.5 mm in diameter and 13 mm in thickness. For this operation a V-shaped joint/weld (edge) preparation was used (Fig. 1). This research is devoted to the welding pass of the talent (called root pass) because of its importance from the point of view of the resistance of the structure to be assembled (Fig. 2) shows an overview of the welding operation of two pipes using the SMAW process.

Two types of materials were used in this research for the tube a steel of type: API 5L X70, and for the filler material (the coated electrode) – a material of type: E6010. The chemical composition of these two materials is presented in Table 1.

The parameters of the real weld on the pipeline are shown in Table 2. The choice of parameters is linked to the geometry of the weld edge preparation in order to avoid lack of fusion (Fig. 3).

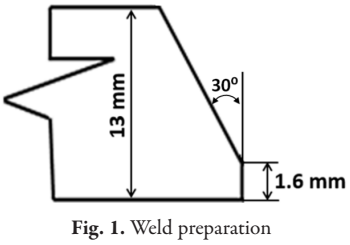

Fig. 1. Weld preparation

ISSN-L 2664-9969; E-ISSN 2706-5448

Fig. 2. General description of the SMAW welding operation

Table 1

Chemical composition of the base metal and of the electrode (% in weight)

Materials	Chemical composition (wt. %)										
	C	Ni	Ti	S	P	Cu	Mn	Si	V	Cr	Fe
Base metal	0.07	0.05	0.04	0.003	0.013	0.03	1.58	0.29	0.06	0.05	Bal
Electrode	0.13	0.07	0.013	0.010	0.006	0.04	0.43	0.20	0.007	0.05	Bal

Table 2

Operating parameters of SMAW welding

Parameters	Values
Welding speed V_s, mm/s	2
Intensity I, A	120
Tension T, V	30
Diameter of electrode D, mm	3.25
Polarity	CC-E

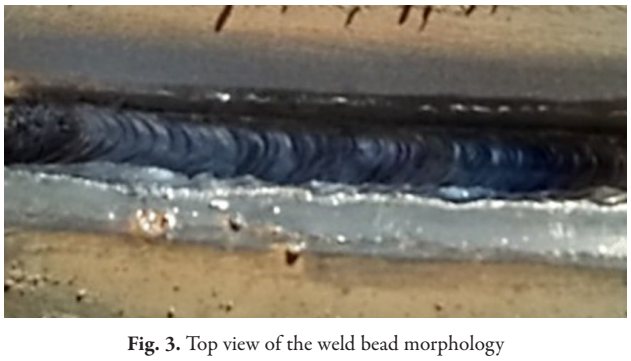

Fig. 3. Top view of the weld bead morphology

2.2. Development of the direct model

2.2.1. Phenomenological analysis

The phenomenological analysis helps in the choosing of equivalent source model(s) (Fig. 4). Indeed, the description of the heat source(s) must take into account the following physical phenomena: The role of the SMAW welding process is to deposit metal that fills the chamfer. It is possible to consider that its chief role is to provide a volumetric energy deposit. However, it must be stressed that the energy provided by the SMAW process comes from the electric arc and the molten metal. This analysis will allow to orientate our choice concerning the modelling of the heat input by the SMAW welding process.

The transverse macrograph shown in (Fig. 5) is the first piece of data to inform about the morphology of the melt zone (shape and size of the melt zone). It allows, on the one hand, to be guided as to the choice of equivalent heat sources, in order to validate the developed numerical model and on the other hand, to study the quality of the weld beads in terms of defects such as: cracks, pores and lack of fusion. The enlarged shape at the bottom of the melt zone is probably related to hydrodynamic movements of the melt pool [25].

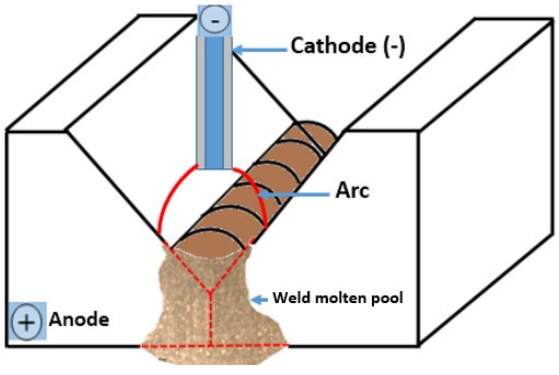

Fig. 4. Principle of the SMAW welding process

To reveal the microstructure, the sample is etched with a widely-used etchant for steels: 4% Nit al. This is a solution composed of 96% ethanol C_2H_5OH and 4% nitric acid HNO_3. The most common method is to immerse the sample in this chemical solution. Etching time varies from 15 to 20 seconds at room temperature, depending on the state of the sample.

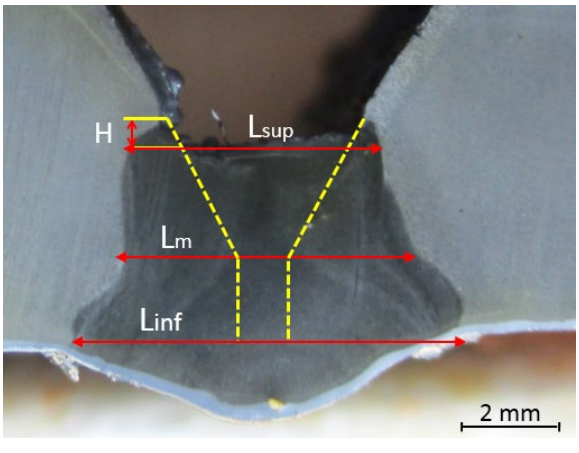

Fig. 5. Macrograph of a weld bead from the first pass obtained by the SMAW

In this work, a model of equivalent heat sources was experimented in order to describe the different phenomena that occur during welding operations.

The model is a combination of three types of heat sources: the first one is a parietal Gaussian surface source on the top face, the second is a Gaussian volume source distributed in the thickness in a conical shape [1]. The third being a Gaussian surface source on the bottom side.

2.2.2. Direct model

A direct model is developed for the manual metal-arc welding process (SMAW) under the COMSOL Multiphysics software (Developer: COMSOL AB, Country of Origin: Sweden, Stockholm). The numerical model is constructed from the heat diffusion equation and the boundary conditions on the different faces of the part. In order to reduce the calculation time, only half of the workpiece was modelled. During welding, the heat input is considered to be constant, and the temperature field is also constant in the arc frame. It is possible to solve the heat diffusion equation in quasi-stationary mode. The computational time is thus greatly reduced compared to a solution in non-stationary mode.

Let's consider a predefined weld metal deposition with a deposit height determined experimentally using macrographs (Fig. 6).

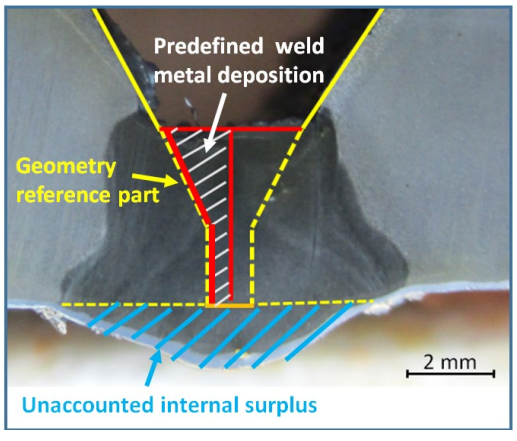

Fig. 6. Deposition of predefined weld metal

2.2.3. Thermophysical properties

In this research it was, it was chosen to apply an evolution of the thermo-physical properties (thermal conductivity, density and latent heat) as a function of temperature. The thermal and mechanical properties of the API 5L X70 steel were defined as a function of the temperature (Fig. 7) [27, 28]. The same properties for both the base material and the weld metal were used in this modeling hypothesis.

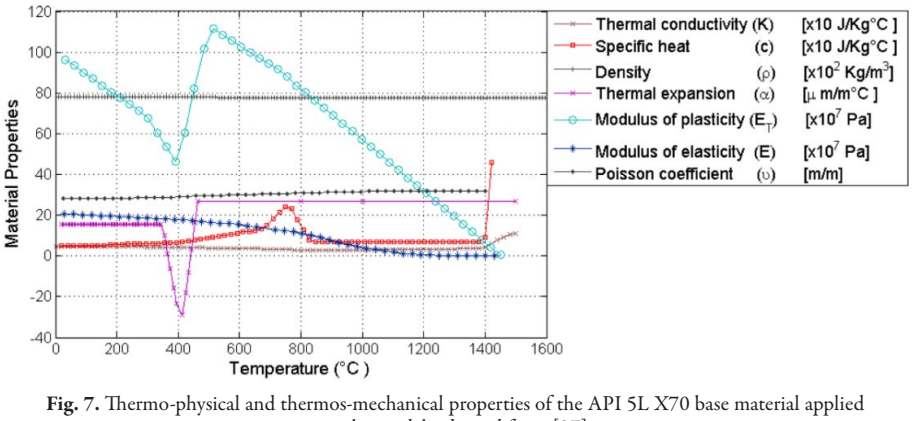

Fig. 7. Thermo-physical and thermos-mechanical properties of the API 5L X70 base material applied to the model, adopted from [27]

2.2.4. Quasi-stationary modelling

The phenomena involved in the various welding processes are transient. However, modelling under these conditions is very costly in terms of memory and calculation time. Moreover, if to use multiphysics calculations it increases the difficulties. One solution to overcome this problem is to model the phenomena in a quasi-steady state or moving reference frame. This resolution has the advantage of indirectly taking into account the transient phenomenon by performing a change of reference frame which will have the effect of moving at the speed of the part. During welding, as the heat input is considered constant, the temperature field is also constant in the electric arc reference frame. Quasi-stationary modelling gives a response at a given time when the regime is stable. This change of reference frame leads to a modification of the heat equation. This formulation can be presented as follows for the case where the source moves along the x axis.

The temperature distribution is calculated by solving the following heat diffusion equation [5]

$$\rho(T)\cdot c_p(T)\cdot V_s\cdot\frac{\partial T}{\partial x}=div\left(\lambda(T)\cdot gradT\right)+Q_{vol}(x,y,z), \quad (1)$$

where ρ – density as a function of temperature; c_p – heat capacity as a function of temperature; V_s – welding speed; T – temperature; λ – conductivity as a function of temperature; Q_{vol} – equivalent volumetric heat source.

The term on the left-hand side of the equation will be directly incorporated into the source term of the part sub domain and corresponds to the convective term. The middle term corresponds to the conductive phenomena and the one on the right-hand side to the source term.

2.2.5. Geometry and thermal boundary conditions

The geometry used is based on that of the experimental model (Fig. 8).

The boundary conditions on the different faces of the part are presented by the following three questions [5]:

– on the faces 1

$$\frac{\partial T}{\partial y}=0, \quad (2)$$

where $\partial T/\partial x$ – the partial derivative of temperature T with respect to the y-direction;

– on the faces 2, 3

$$-\lambda\cdot\frac{\partial T}{\partial z}=h\left(T-T_{inf}\right)+q_{surf}; \quad (3)$$

– on the faces 4

$$-\lambda\cdot\frac{\partial T}{\partial n}=h\left(T-T_{inf}\right), \quad (4)$$

where λ – conductivity; h – exchange coefficient; T – temperature; T_{inf} – initial temperature; q_{surf} – surface heat source.

The exchange coefficient h used in the boundary conditions and the globalization of convective and radiative transfers is presented by the following equation [28]

$$h=24.1\cdot10^{-4}\varepsilon T^{1.61}, \quad (5)$$

where ε – emissivity of 0.4.

Modeling heat input using the equivalent source approach is based on reproducing the shape of the melted zone as closely as possible to reality.

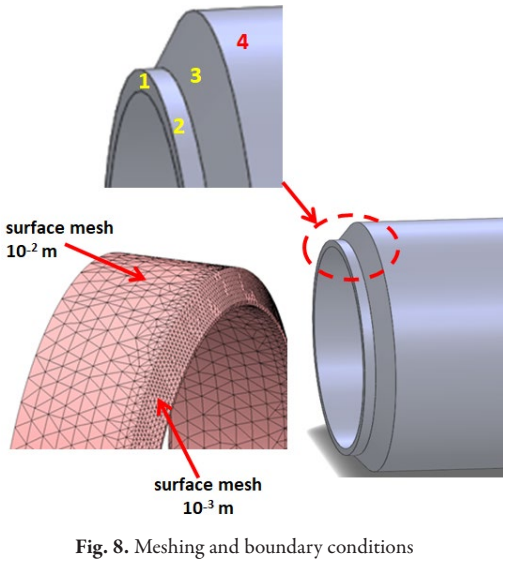

Fig. 8. Meshing and boundary conditions

ISSN-L 2664-9969; E-ISSN 2706-5448

The closer the numerical melt zone is to the experimental melt zone. The numerical model can accurately describe the temperature changes caused by welding operations. A priori, each welding process gives a different shape to the melted zone. These differences are due to a number of factors: type of energy, type of shielding gauze, welding speed, etc. In this case, SMAW welding of the tubes gave a different shape than tubes studied previously. This shape can be broken down into three parts (Fig. 9): the first part is a widening of the bath on the upper side, probably due to the effect of the electric arc. The second part is a conical shape in the form of volume energy due to the addition of molten material. The last part is another widening on the lower side of the weld, probably due to the hydrodynamic movements of the molten bath. This analysis led to select three types of heat sources in order to recover the same shape of the melt zone from the macrographs [28].

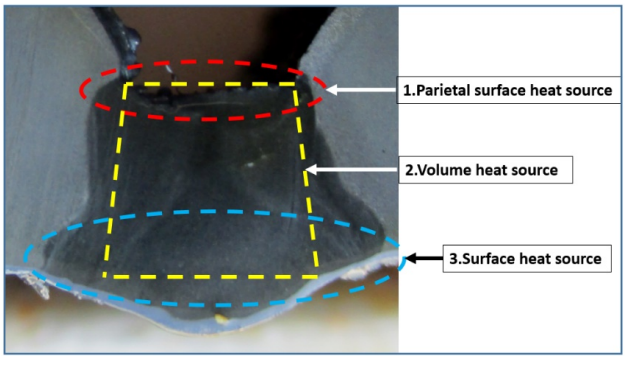

Fig. 9. Description of the effective range of the three heat sources in relation to the transverse macrography

2.2.6. Source terms

The choice of sources is based on a combination of three types of heat sources: the first is a Gaussian parietal source represented by the following equation

$$q_{surf\_sup}(x,y,z)=\frac{E\eta_1}{2\pi r_{surf\_sup}^2}\cdot e^{\left(-\left(\frac{x^2+y^2}{2r_{surf\_sup}^2}\right)\right)}e^{\left(-\frac{z^2}{dz^2}\right)}, \quad (6)$$

where E – energy of the electric arc; η_1 – fraction of the top-side surface source yield; r_{surf_sup} – radius of the top surface source; dz – penetration depth of the parietal distribution.

The second is Gaussian volume source distributed through the thickness in a conical shape represented by the following equation [1]

$$Q_{vol}(x,y,z)=\frac{9E\eta_2}{\pi h\left(r_0^2+r_0r_1+r_1^2\right)}e^{\left(-3\frac{x^2+y^2}{r_z^2}\right)[1-u(z+h)]}, \quad (7)$$

where E – energy of the electric arc; η_2 – fraction of the volume source yield; r_0 – radius of fusion at $z = 0$; r_1 – radius of fusion in $z = -h$; h – thickness of the bead to be welded (penetration depth).

The third is Gaussian surface source (expansion of the pool on the lower side), this shape is described by the following equation

$$q_{surf\_inf}(x,y)=\frac{E\eta_3}{2\pi r_{surf\_inf}^2}e^{\left(-\left(\frac{x^2+y^2}{2r_{surf\_inf}^2}\right)\right)}, \quad (8)$$

where E – energy of the electric arc; η_3 – fraction of surface heat source efficiency bottom side; r_{surf_inf} – radius of the surface source bottom side.

Table 3 presents all the input parameters of the equivalent heat source model.

Table 3

Parameter values of the equivalent heat sources of the central point

Parameters	Value
First source of heat	
E, W	3600
η_1	0.25
r_{surf_sup}, mm	2.4
dz, mm	0.57
Second source of heat	
E	3600
η_2	0.50
r_0	3
r	1.5
h	4
Third source of heat	
E	3600
η_3	0.25
r_{surf_inf}	4

2.3. Optimization using a numerical design of experiments (NDE)

2.3.1. Implementation of the numerical design of experiments

The difficulties associated with identifying the parameters of equivalent sources led to use a method of parameter optimization that is both simple to implement and robust: the numerical design of experiments (NDE) method. It allows the estimation, with a limited number of calculations, of the effects of the model influence factors (parameters of the analytical expressions of the equivalent heat sources) on the objective functions (characteristics of the numerical melt zone). In this research, three equivalent source parameters (r_{surf_sup}, r_{sur_inf}, r_0), thermal conductivity λ and four objective functions were chosen. These functions are the width of the upper part (L_{sup}), the width of the central part (L_m), the width of the lower part of the molten zone (L_{inf}) and the height of the deposit on the chamfered walls (H). In the literature, there are several studies that address the modelling of welding operations. Fig. 10 shows a flowchart of the algorithm for solving the parameter sensitivity problem using the NED method.

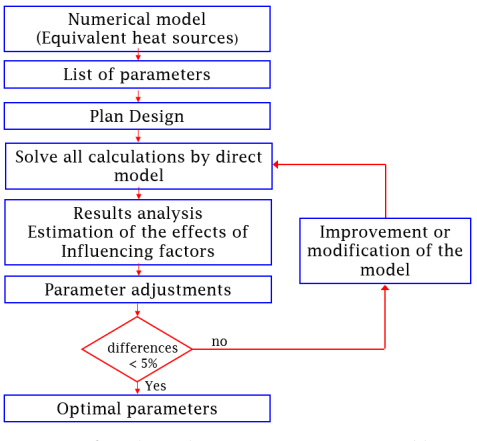

Fig. 10. Diagram for solving the parameter sensitivity problem using the Numerical Design of Experiments method

2.3.2. Objective functions (OF)

In order to characterize the shape of the molten zone numerically, four objective functions L_{inf}, L_m, L_{sup} and H (Fig. 11) were chosen:

- L_{inf}: width of the molten area on the bottom side;
- L_m: width in the middle of the bead;
- L_{sup}: width of the molten area on the upper side;
- H: height of the deposit on the chamfer walls.

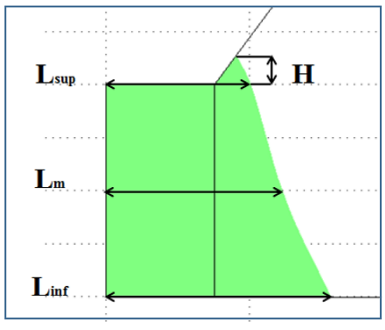

Fig. 11. Presentation of the objective functions

2.3.3. Influencing factors (IF)

Three equivalent heat source parameters were chosen to study: r_{sur_inf}, r_{sur_sup} and r_0, and the thermal conductivity λ (w/m · k). Table 4 shows the four parameters with their ranges of variation. The four parameters represent influencing factors for the study carried out by the numerical design method. The range of variation of each parameter is chosen in such a way as to obtain (in the case of through-welding) plausible shapes of the melted areas. The boundaries of the chosen ranges for the 4 factors are the lower and upper levels assigned to the influencing factors in the program matrix of the numerical experimental design (Table 5).

The experimental design chosen is of the CED 2^4 type (complete experimental design, with 16 trials, for 4 influence factors, each with two levels). The calculations of the objective function values were carried out using the numerical model and following the program matrix. For each of the 16 numerical "trials" in the experimental design, the values in each row of the program matrix were assigned to the model parameters (IF), which allowed the values of the objective functions to be calculated. 16 simulation calculations were thus carried out using the model and following the NED. The total calculation time was 60 minutes.

Table 4

Influencing factors and their levels of variation

Influencing factors	Range of variation
Radius of the surface source top face r_{surf_sup}, mm	[1.4; 3.4]
Radius of the surface source bottom side r_{surf_inf}, mm	[3; 5]
Radius side top of the volume source r_0, mm	[2; 4]
Conductivity: λ, w/m · k	[48; 52]

2.3.4. Program matrix (PM)

The program matrix for the selected numerical conditions (4 influence factors with 2 levels and four objective functions) consists of 16 trials (24 trials) [29–31]. The coded and physical levels of the influence factors as well as the measured values of the objective functions (L_{inf}, L_m, L_{sup} and H) are presented in Table 5.

It is noted in Table 5 that the results of the different objective functions have positive values, except for the H value from test number 12. The usefulness of these numerical plans, on the one hand, is to quantify the influence of the model parameters on the chosen Objective Functions, in order to minimize the number of parameters to be studied, and on the other hand, try to find the range of input parameters of the model, in order to judge the robustness of the digital model.

Table 5

Program matrix (PM)

No. trials	Influence factors								Objective functions			
	Coded values				Physical values							
	r_{surf_sup}	r_{surf_inf}	r_0	λ	r_{surf_sup}, mm	r_{surf_inf}, mm	r_0, mm	λ, w/m · k	L_{sup}	L_m	L_{inf}	H
1	−1	−1	−1	−1	1.4	3	2	48	3.15	3.8	4.38	0.96
2	+1	−1	−1	−1	3.4	3	2	48	2.64	3.46	4.2	0.20
3	−1	+1	−1	−1	1.4	5	2	48	2.72	3.05	3.82	0.63
4	+1	+1	−1	−1	3.4	5	2	48	2.16	2.56	3.5	0.01
5	−1	−1	+1	−1	1.4	3	4	48	3.50	4.15	4.63	1.21
6	+1	−1	+1	−1	3.4	3	4	48	3.14	3.9	4.5	0.84
7	−1	+1	+1	−1	1.4	5	4	48	3.10	3.52	4.3	0.92
8	+1	+1	+1	−1	3.4	5	4	48	2.60	3.2	4.1	0.43
9	−1	−1	−1	+1	1.4	3	2	52	2.71	3.3	3.95	0.60
10	+1	−1	−1	+1	3.4	3	2	52	2.21	2.9	3.8	0.18
11	−1	+1	−1	+1	1.4	5	2	52	2.32	2.42	3.12	0.30
12	+1	+1	−1	+1	3.4	5	2	52	1.81	1.9	2.7	0.00
13	−1	−1	+1	+1	1.4	3	4	52	3.00	3.65	4.2	0.85
14	+1	−1	+1	+1	3.4	3	4	52	2.60	3.4	4.1	0.44
15	−1	+1	+1	+1	1.4	5	4	52	2.65	2.95	3.6	0.55
16	+1	+1	+1	+1	3.4	5	4	52	2.15	2.5	3.35	0.09

3. Results and Discussion

3.1. Results of the comparison between the thermal model and the macrographs

The equivalent heat sources used in this research were able to faithfully reproduce the shape of the experimental molten zone from a SMAW electric arc welding operation. The numerical calculation in COMSOL multiphysics allowed the extraction of two types of information, the first one is the shape of the geometry of the melted zone and the second one is the temperature gradients in the workpiece (Fig. 12).

Validation of the numerical model: A comparative study of the measurements of the simulated molten zone and that observed experimentally is necessary to test the relevance of the response of the model developed. The validation of this calculation is obtained by comparing the dimensions, L_{sup}, L_m, L_{inf} and H taken from the transverse macrographic section.

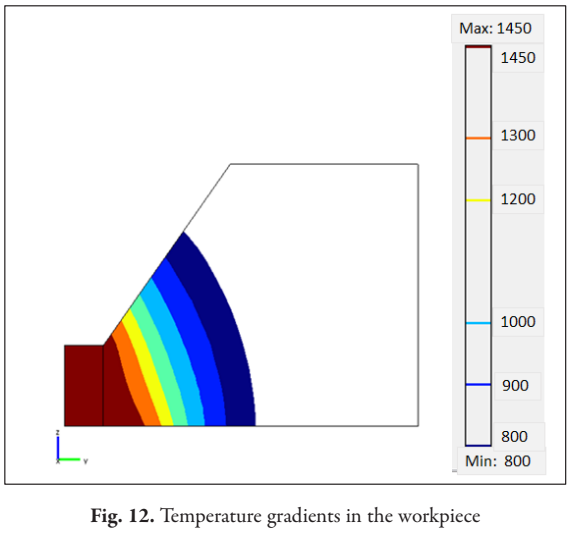

Fig. 12. Temperature gradients in the workpiece

ISSN-L 2664-9969; E-ISSN 2706-5448

In this case, let's note a good agreement between the direct model and the dimensions recorded on the macrographic sections, except for the measure L_m, where let's note a deviation between the measurements and the model of 11.4% (Table 6). This discrepancy leads to implement a method of optimization (adjustment) of the input parameters of the model.

Table 6

Comparison between experimental geometry and the numerical model

Measurements	Experiment	Model	Deviation (%)
L_{sup}, mm	2.74	2.67	2.50
L_m, mm	3.05	3.40	11.40
L_{inf}, mm	3.91	4.14	5.80
H, mm	0.57	0.55	3.50

Note: the line colored in orange shows a significant discrepancy of 11.4% between the measurements and the model

3.2. Results of the analysis of the model's behavior in relation to heat source parameters

The results obtained by the direct model (Table 6) are satisfactory, with the exception of the Lm dimension, for which there is a relative difference of 11.4% between the calculations and the measurements. In this case the objective of obtaining a deviation of less than 5% between the values measured on the macrographs and the values calculated by the model with the parameter sets (Table 4) is not achieved. Later, a detailed explanation of the measures taken to adjust the parameter(s) in order to reduce the 11.4% gap without significantly altering the other objective functions.

The analysis of the results of the numerical design of experiments allowed to estimate the effects of the 4 influencing factors (model parameters) on the 4 objective functions (characteristics of the molten zone) and to draw the effect diagrams (PARETO diagrams) (Fig. 13–16). The analysis of the effects diagrams allows to make the following comments:

– the factor r_{surf_sup} is the most influential on H, and L_{sup} (Fig. 13, 16), and its influence is "inverse": if r_{surf_sup} increases, H, and L_{sup} decrease;
– the factor λ (Lambda) also influences L_{sup}, L_m and L_{inf}; its influence is direct for L_{inf} and inverse for L_{sup}, L_m: if λ increases, L_{inf} increases, but Ls_{up}, L_m decrease;
– the dimensions L_m and L_{inf} (Fig. 14 and 15), are mainly influenced by r_{surf_inf}, and its influence is "inverse": if r_{surf_inf} decreases, L_m, and L_{inf} increase.

The magnitude and direction of the estimated effects of influencing factors (IF) on objective functions are known. The acquisition of information is necessary to determine which IFs need to be adjusted in order to simultaneously achieve the "target" values of the objective functions OF. In our case, the target values of the objective functions are the measured values.

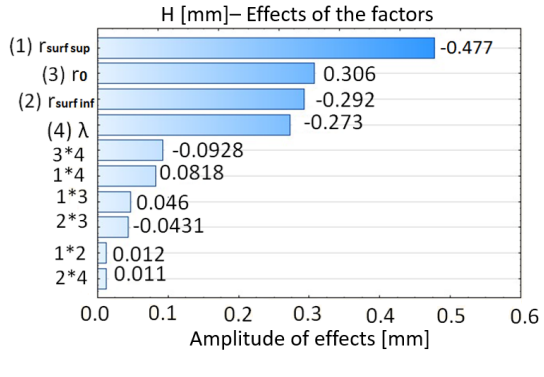

Fig. 13. Influence of the factors on the height of the deposit H, mm

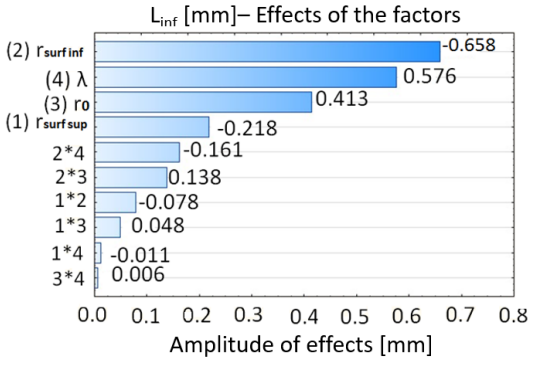

Fig. 14. Influence of the factors on the width of the melted area on the lower side L_{inf}, mm

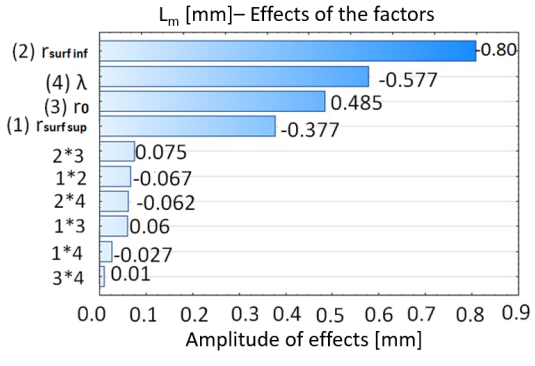

Fig. 15. Influence of the factors on the width in the middle of the weld bead L_m, mm

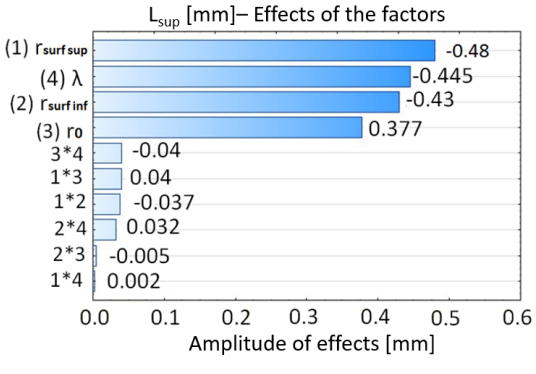

Fig. 16. Influence of the factors on the width of the melted area on the upper side L_{sup}, mm

3.3. Results of the model's optimal parameters

3.3.1. Adjustment of the model parameters

The effects diagram allows the parameters of the numerical model to be adjusted in order to bring the calculated values closer to the measured values. Taking into account, on the one hand, the magnitude. And direction of the effects of the influencing factors on the objective functions. And on the other hand, taking care not to affect the values of the calculated objective functions. The initial values in Table 6 were used.

In order to reduce the discrepancy between measurements and calculations, for the dimension L_m, with less consequence on other objective functions, It is possible to choose as initial values those grouped in Table 4. It is proposed to perform the adjustment using the parameter r_{surf_inf} which has an important influence on width in the middle of the bead (L_m). To increase the width at the middle of the bead L_m, the adjustment (Table 7) consists in increasing the dimension r_{surf_inf} by 0.5 of its value at the central point. Then the L_m value changes from 3.25 to 3.09 mm. The other objective functions are affected by this change, but they remain within the confidence interval of the measurements.

Table 7

Parameter sets used for the method

Trial	Influence factors				Objective functions			
	r_{surf_sup}, mm	r_{surf_inf}, mm	r_0, mm	λ, w/m · k	L_{sup}, mm	L_m, mm	L_{inf}, mm	H, mm
PC	2.4	4	3	50	2.67	3.25	4.15	0.55
Adjustment	1.4	**4.5**	3	50	2.68	3.09	3.93	0.58

Note: the value colored in red shows the modification of the r_{surf_inf} parameter value from 4 to 4.5 mm

3.3.2. Validation of the numerical model

Validation of the numerical model is based on macrographic sections. Some model parameters are modified. The weld bead geometry obtained in SMAW welding was correctly reproduced by the model (Fig. 17).

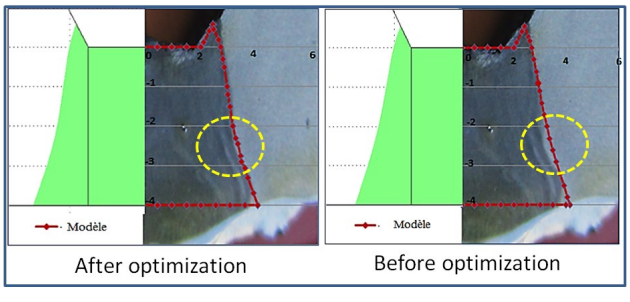

Fig. 17. Comparison between the experimental geometry and the numerical model before and after optimization

Fig. 17 shows the comparison of the shapes of the measured and calculated melt zones using the adjusted parameters (Table 7). A very good agreement between the measurements and model is observed.

A slight difference was noted between the experimental and numerical results of just fewer than 2.1% (Table 8).

Table 8

Comparison dimensions (experiments – model) after optimization

Magnitude	Measurements	Direct model	Deviation (%)	Adjustment	Deviation (%)
L_{sup}, mm	2.74	2.67	2.50	2.68	2.1
L_m, mm	3.05	3.25	11.40	3.09	1.2
L_{inf}, mm	3.91	4.15	5.80	3.93	0.5
H, mm	0.57	0.55	3.50	0.58	1.7

In several researches already cited in section 1, the method for selecting equivalent heat source parameters is not clearly identified. In contrast, in our research, the choice of source parameter values is clearly presented. Furthermore, the equivalent heat source approach requires particular care in adjusting the parameters to reduce the discrepancy between the model and the experiment. To this end, the method developed here allows for the effective and relevant adjustment of the parameters.

Optimizing the parameters integrated into the numerical model is very important for validating numerical models. There are several optimization methods available for this purpose. The difficulty in using each method lies in its implementation and selection. As part of this work, an approach is adapted that is both simple to implement and delivers excellent results in terms of optimization. This approach can be applied to several processes in different fields that have a number of important parameters. An important factor in using this approach is:

- the choice of optimized input parameters (which are likely to have an influence);
- the output functions;
- the levels of the various parameters;
- the type of digital plans;
- the interpretation of the results.

The limitations of the proposed research lie in the use of a single source of information, namely macrographs, for the validation of numerical models. In order to eliminate these limitations, it is recommended to use other characterization methods such as: thermocouples to obtain temperature field changes; visualization of molten pools using a high-speed camera to obtain molten pool lengths in real time.

In this research, the results obtained can be used to model electric arc welding operations on pipelines. The values obtained can be integrated into models with similar configurations. However, the results obtained here are not valid for other welding processes and other configurations. On the other hand, the approach developed in this work remains reliable for all types of welding processes.

4. Conclusions

1. Macrography allows to study the shape of the melted area. Thanks to phenomenological analysis, it is succeeded in accurately reproducing the shape of the melted area using mathematical expressions (heat source concept) with a direct model. The results show good agreement between the direct model and the dimensions recorded on the macrographic sections, with the exception of the measurement of the width at the center of the L_m cord.
2. The results of the numerical design of experiments show that, the dimension width in the middle of the bead (L_m) are mainly influenced by radius of the surface source bottom side (r_{surf_inf}), and its influence is "inverse": if r_{surf_inf} decreases L_m increase. And that, if r_{surf_inf} varies from 3 to 5 mm, the width L_m decreases by 0.8 mm.
3. Adjusting the r_{surf_inf} factor by 0.5 from its value at the center point allows the Lm value to change from 3.25 mm to 3.09 mm. This adjustment optimizes the digital model by improving it and reducing the discrepancy between the simulation and the experiment for the L_m function from 11.4% to 1.2%.

Conflict of interest

The authors declare that they have no conflict of interest in relation to this research, including financial, personal, authorship or other, which could affect the research and its results presented in this article.

Financing

The research was performed without financial support.

Data availability

The manuscript has no linked data.

Use of artificial intelligence

The authors confirm that they did not use artificial intelligence technologies in creating the submitted work.

ISSN-L 2664-9969; E-ISSN 2706-5448

Authors' contributions

Adel Chouiter: Conceptualization, Methodology, Formal analysis, Resources; ***Lyes Bidi***: Conceptualization, Methodology, Writing – original draft; ***Hadjer Bensiali***: Conceptualization, Methodology, Formal analysis, Resources; ***Rachid Chaib***: Conceptualization, Methodology, Writing – review and editing; ***Philippe Le Masson***: Conceptualization, Methodology.

References

1. Goldak, J., Chakravarti, A., Bibby, M. (1984). A new finite element model for welding heat sources. *Metallurgical Transactions B, 15 (2),* 299–305. https://doi.org/10.1007/bf02667333
2. Yu, D., Yang, C., Sun, Q., Dai, L., Wang, A., Xuan, H. (2023). Impact of process parameters on temperature and residual stress distribution of X80 pipe girth welds. *International Journal of Pressure Vessels and Piping, 203,* 104939. https://doi.org/10.1016/j.ijpvp.2023.104939
3. Kong, F., Ma, J., Kovacevic, R. (2011). Numerical and experimental study of thermally induced residual stress in the hybrid laser-GMA welding process. *Journal of Materials Processing Technology, 211 (6),* 1102–1111. https://doi.org/10.1016/j.jmatprotec.2011.01.012
4. Liu, S., Sun, J., Wei, F., Lu, M. (2018). Numerical simulation and experimental research on temperature and stress fields in TIG welding for plate of RAFM steel. *Fusion Engineering and Design, 136,* 690–693. https://doi.org/10.1016/j.fusengdes.2018.03.058
5. Bidi, L., Mattei, S., Cicala, E., Andrzejewski, H., Le Masson, P., Schroeder, J. (2011). The use of exploratory experimental designs combined with thermal numerical modelling to obtain a predictive tool for hybrid laser/MIG welding and coating processes. *Optics & Laser Technology, 43 (3),* 537–545. https://doi.org/10.1016/j.optlastec.2010.07.011
6. Zubairuddin, M., Albert, S. K., Vasudevan, M., Mahadevan, S., Chaudhari, V., Suri, V. K. (2017). Numerical simulation of multi-pass GTA welding of grade 91 steel. *Journal of Manufacturing Processes, 27,* 87–97. https://doi.org/10.1016/j.jmapro.2017.04.031
7. Bendaoud, I., Matteï, S., Cicala, E., Tomashchuk, I., Andrzejewski, H., Sallamand, P. et al. (2014). The numerical simulation of heat transfer during a hybrid laser–MIG welding using equivalent heat source approach. *Optics & Laser Technology, 56,* 334–342. https://doi.org/10.1016/j.optlastec.2013.09.007
8. Obeid, O., Alfano, G., Bahai, H., Jouhara, H. (2018). Numerical simulation of thermal and residual stress fields induced by lined pipe welding. *Thermal Science and Engineering Progress, 5,* 1–14. https://doi.org/10.1016/j.tsep.2017.10.005
9. Goldak, J., Bibby, M., Moore, J., House, R., Patel, B. (1986). Computer modeling of heat flow in welds. *Metallurgical Transactions B, 17 (3),* 587–600. https://doi.org/10.1007/bf02670226
10. Li, W., Yu, R., Huang, D., Wu, J., Wang, Y., Hu, T. et al. (2019). Numerical simulation of multi-layer rotating arc narrow gap MAG welding for medium steel plate. *Journal of Manufacturing Processes, 45,* 460–471. https://doi.org/10.1016/j.jmapro.2019.07.035
11. Pichot, F., Danis, M., Lacoste, E., Danis, Y. (2013). Numerical definition of an equivalent GTAW heat source. *Journal of Materials Processing Technology, 213 (7),* 1241–1248. https://doi.org/10.1016/j.jmatprotec.2013.01.009
12. Danis, Y., Lacoste, E., Arvieu, C. (2010). Numerical modeling of inconel 738LC deposition welding: Prediction of residual stress induced cracking. *Journal of Materials Processing Technology, 210 (14),* 2053–2061. https://doi.org/10.1016/j.jmatprotec.2010.07.027
13. Farias, R. M., Teixeira, P. R. F., Vilarinho, L. O. (2021). An efficient computational approach for heat source optimization in numerical simulations of arc welding processes. *Journal of Constructional Steel Research, 176,* 106382. https://doi.org/10.1016/j.jcsr.2020.106382
14. Lei, Y., Zhu, Q., Zhang, L., Gu, K., Ju, X. (2010). Simulation on the welding of CLAM steel. *Fusion Engineering and Design, 85 (7–9),* 1503–1507. https://doi.org/10.1016/j.fusengdes.2010.04.014
15. Bag, S., Trivedi, A., De, A. (2009). Development of a finite element based heat transfer model for conduction mode laser spot welding process using an adaptive volumetric heat source. *International Journal of Thermal Sciences, 48 (10),* 1923–1931. https://doi.org/10.1016/j.ijthermalsci.2009.02.010
16. Flint, T. F., Francis, J. A., Smith, M. C., Balakrishnan, J. (2017). Extension of the double-ellipsoidal heat source model to narrow-groove and keyhole weld configurations. *Journal of Materials Processing Technology, 246,* 123–135. https://doi.org/10.1016/j.jmatprotec.2017.02.002
17. Chen, L., Mi, G., Zhang, X., Wang, C. (2019). Numerical and experimental investigation on microstructure and residual stress of multi-pass hybrid laser-arc welded 316L steel. *Materials & Design, 168,* 107653. https://doi.org/10.1016/j.matdes.2019.107653
18. Farias, R. M., Teixeira, P. R. F., Vilarinho, L. O. (2022). Variable profile heat source models for numerical simulations of arc welding processes. *International Journal of Thermal Sciences, 179,* 107593. https://doi.org/10.1016/j.ijthermalsci.2022.107593
19. Mondal, A. K., Kumar, B., Bag, S., Nirsanametla, Y., Biswas, P. (2021). Development of avocado shape heat source model for finite element based heat transfer analysis of high-velocity arc welding process. *International Journal of Thermal Sciences, 166,* 107005. https://doi.org/10.1016/j.ijthermalsci.2021.107005
20. Belitzki, A., Marder, C., Huissel, A., Zaeh, M. F. (2016). Automated heat source calibration for the numerical simulation of laser beam welded components. *Production Engineering, 10 (2),* 129–136. https://doi.org/10.1007/s11740-016-0664-9
21. Gannon, L., Liu, Y., Pegg, N., Smith, M. (2010). Effect of welding sequence on residual stress and distortion in flat-bar stiffened plates. *Marine Structures, 23 (3),* 385–404. https://doi.org/10.1016/j.marstruc.2010.05.002
22. Azadi Moghaddam, M., Golmezergi, R., Kolahan, F. (2016). Multi-variable measurements and optimization of GMAW parameters for API-X42 steel alloy using a hybrid BPNN–PSO approach. *Measurement, 92,* 279–287. https://doi.org/10.1016/j.measurement.2016.05.049
23. García-García, V., Reyes-Calderón, F., Camacho-Arriaga, J. C. (2016). Optimization of experimental temperature measurement in GTAW process by means of DoE technique and computational modeling. *Measurement, 88,* 297–309. https://doi.org/10.1016/j.measurement.2016.03.049
24. Fu, G., Gu, J., Lourenco, M. I., Duan, M., Estefen, S. F. (2014). Parameter determination of double-ellipsoidal heat source model and its application in the multi-pass welding process. *Ships and Offshore Structures, 10 (2),* 204–217. https://doi.org/10.1080/17445302.2014.937059
25. Bidi, L., Le Masson, P., Cicala, E., Primault, C. (2017). Experimental design method to the weld bead geometry optimization for hybrid laser-MAG welding in a narrow chamfer configuration. *Optics & Laser Technology, 89,* 114–125. https://doi.org/10.1016/j.optlastec.2016.09.046
26. Wang, H., Woo, W., Kim, D.-K., Em, V., Lee, S. Y. (2018). Effect of chemical dilution and the number of weld layers on residual stresses in a multi-pass low-transformation-temperature weld. *Materials & Design, 160,* 384–394. https://doi.org/10.1016/j.matdes.2018.09.016
27. Forouzan, M. R., Heidari, A., Golestaneh, S. J. (2009). FE simulation of submerged arc welding of API 5L-X70 straight seam oil and gas pipes. *Journal of Computational Methods in Engineering, 28,* 93–110 Available at: https://jcme.iut.ac.ir/article_3029_3925785f0e7afbb5933eb87d589edb33.pdf
28. Bensiali, H., Bidi, L., Cicala, E., Le Masson, P., Chibani, M. E. B., Boulahlib, M. S. (2021). Effects of operating parameters on weld bead morphology with welding operations of API 5L X70 steel pipes by SMAW process. *Welding in the World, 65 (6),* 1119–1129. https://doi.org/10.1007/s40194-021-01085-4
29. Bidi, L., Le Masson, P., Cicala, E. (2024). Influences of laser on the energy parameters of the electric arc in the case of laser-MIG hybrid welding. *The International Journal of Advanced Manufacturing Technology, 131 (7–8),* 4055–4069. https://doi.org/10.1007/s00170-024-13244-0
30. Goupy, J. (2001). *Introduction aux plans d'expériences.* Paris: Dunod. Available at: https://iadji.com/wp-content/uploads/2020/08/Introduction-aux-Plans-dExperiences.pdf
31. Montgomery, D. C. (1991). *Design and analysis of experiments.* Singapore: John Wiley & Sons. Available at: https://www.scribd.com/document/405637459/Douglas-C-Montgomery-Design-and-analysis-of-experiments-Wiley-1991-pdf?language_settings_changed=English

Adel Chouiter, *PhD in Mechanical Engineering, HDR, Department of Mechanical Engineering, Laboratory Applied Sciences of Mechanics, Electromechanics and Materials (ASMEM), Mentouri Brothers University Constantine1, Constantine, Algeria, ORCID: https://orcid.org/0009-0003-1064-1805*

Lyes Bidi, *PhD in Mechanical Engineering, Professor, Laboratory Applied Sciences of Mechanics, Electromechanics and Materials (ASMEM), Mentouri Brothers University Constantine1, Constantine, Algeria, ORCID: https://orcid.org/0000-0003-0621-1274*

Hadjer Bensiali, *Doctor of Technical Sciences, PhD, Department of Transport Engineering, Laboratory of Transports and Environment Engineering, Mentouri Brothers University Constantine1, Constantine, Algeria, ORCID: https://orcid.org/0009-0000-9182-5005*

✉***Rachid Chaib,*** *Doctor of Technical Sciences, Professor, Department of Transport Engineering, Laboratory of Transports and Environment Engineering, Mentouri Brothers University Constantine1, Constantine, Algeria, e-mail: r3chaib@yahoo.fr, ORCID: https://orcid.org/0000-0001-8680-1906*

Philippe Le Masson, *PhD in Mechanical Engineering, Professor, C. HUYGENS Research Centre, University of Southern Brittany, Morbihan, France, ORCID: https://orcid.org/0000-0003-2721-8504*

✉*Corresponding author*